Magnetization switching and domain-wall propagation behavior in edge-modulated ferromagnetic nanowire structures

David M. Burn, Erhan Arac, and Del Atkinson*
Department of Physics, Durham University, Durham, DH1 3LE, United Kingdom
(Received 26 March 2013; revised manuscript received 5 September 2013; published 24 September 2013)

The magnetization reversal processes in ferromagnetic nanowires with sinusoidally modulated edges were investigated as a function of modulation amplitude and wavelength. The reversal processes were studied in two regimes: nucleation controlled reversal and magnetization reversal mediated by domain-wall propagation. In the latter case, domain walls were introduced using both nucleation-pad structures and local pulsed-field injection techniques. The reversal behavior shows that competing effects govern the switching fields in these structures, giving a minimum as a function of modulation wavelength, showing promising results for improved control of domain-wall propagation behavior. The experimental results were interpreted with detailed micromagnetic simulations and an analytical model, based on the demagnetization effects of the modulation upon the spin structure of the wire. The analysis highlights consistent trends in the reversal behavior resulting from modulation, and, significantly, the switching behavior is found to be scalable in relation to the amplitude and wavelength.

DOI: 10.1103/PhysRevB.88.104422 PACS number(s): 75.60.Ch, 81.07.Gf, 75.75.−c

I. INTRODUCTION

Magnetization reversal behavior in ferromagnetic nanowire structures has received much attention due to novel spintronic devices envisioned for memory,[1–3] logic,[4] and sensing applications. More recently trapping nanoparticles with localized fields from a domain wall (DW) has led to the development of techniques for the detection[5] and manipulation[6–9] of magnetic nanoparticles and even atoms.[10] This opens possibilities for transporting molecules or biological entities leading to potential for drug delivery, molecular detection, and nanofluidics.

The success of these technologies relies on the understanding of the fundamental magnetization behavior in ferromagnetic nanowires and nanostructures. In particular, the behavior of DWs and techniques for gaining control over their structure and position are of great importance.

Geometrical patterning of thin magnetic films allows control over DWs by producing nanowires as DW conduits.[11] Multiple mechanisms are available for the movement of DWs along nanowires such as the application of a field,[12] through spin-transfer torque,[13] and the interaction with spin waves.[14,15] Nanowire geometry can be manipulated to direct DWs around corners,[16] give control over the propagation direction,[17–19] and artificially pin DWs at specific locations along a nanowire.[16,20–22] Additionally, modification to the edge profile of a nanowire can lead to improvements to the dynamic DW behavior. This was realized in the work by Nakatani *et al*. where an increase in DW mobility was found with increasing edge roughness.[23] Since then, various geometries have given promising results both experimentally[24] and theoretically.[25–28]

These periodic geometrical modifications can fundamentally modify the magnetization process showing improved DW dynamics and control over the depinning field for DWs in the nanowire.[25] In DW-based devices, both improved DW dynamics and control over the pinning and depinning of DWs is desirable. However, little attention has been paid toward a detailed understanding of the initiation of reversal processes and the relationship to the modulation parameters. Depending upon the structure, the magnetic field-driven reversal process in nanowires may occur via direct nucleation of reversal from an initially uniform magnetization state at a relatively high field, or in the presence of a pre-existing DW the reversal is mediated via DW propagation with a relatively low field. Furthermore, the work to date has made little attempt to describe the commonality of behavior or to look for scaling effects associated with the modulation parameters that can provide more generalized physical insight.

Here a detailed experimental and micromagnetic investigation describes the switching field behavior of nanowires with sinusoidal edge structuring on both edges and explains the physical basis for the observed behavior. Specifically, two aspects of the structuring are investigated, namely, (a) switching by the nucleation of a reverse domain followed by DW propagation and (b) the effects that nanowire modulation geometry have upon the pinning and propagation of a pre-existing DW within a nanowire.

II. EXPERIMENTAL

Experimental measurements were performed on edge-modulated planar nanowire structures fabricated on Si/SiO_2 substrates by electron-beam lithography followed by thin-film deposition using thermal evaporation and lift-off. The magnetization reversal behavior was measured using focused longitudinal magneto-optic Kerr effect (MOKE) measurements.[29]

The nanowire structures were typically 20-μm long, had an average width of 250 nm, and were patterned in small arrays of nanowires with a pitch of 800 nm. This increases the signal-to-noise ratio for MOKE measurements giving an averaged behavior over multiple wires to reduce the significance of any local variations while still being representative of an individual noninteracting nanowire.[30] The nanowires were formed by the thermal evaporation of 10-nm NiFe from a single alloy source of nominal composition $Ni_{81}Fe_{19}$ followed by a 2.5-nm Au protective cap deposited without breaking the vacuum. Deposition rates and thicknesses were monitored by an *in situ*

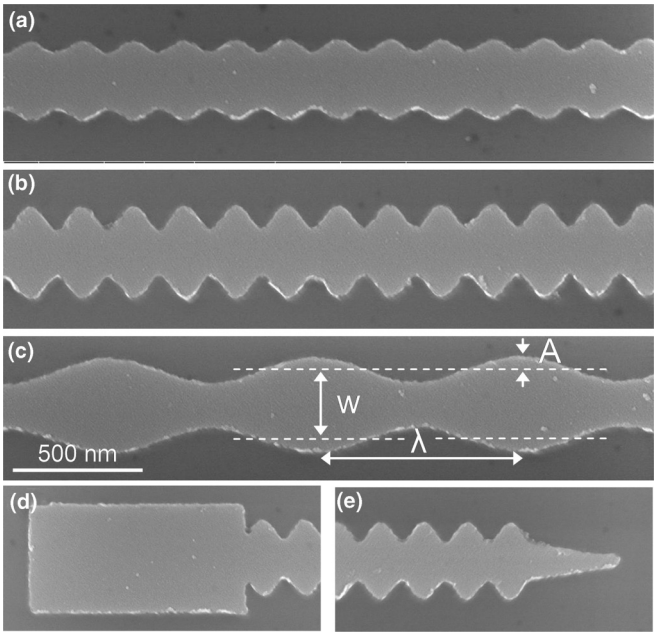

FIG. 1. Scanning electron microscope images of fabricated nanowires with modulation wavelengths, λ, and amplitudes, A, (a) 0.2 μm, 25 nm; (b) 0.2 μm, 50 nm; and (c) 0.8 μm, 50 nm, respectively. The nanowires are terminated with either a (d) DW injection pad or (e) tapered wire section.

quartz rate-monitor, which was previously calibrated by x-ray reflectivity measurements.

Two sets of samples were fabricated to address the two strands of this study. The nanostructures for the nucleation studies consisted of modulated nanowires terminated with 500-nm-long tapered points in order to limit end effects and allow the influence of the modulation on the reversal to be studied.

For the analysis of DW-mediated reversal, a second set of nanowires was prepared with a 1-μm-long, 500-nm-wide DW nucleation pad added to one end of each nanowire to give controlled DW injection.[11] The other end of the nanowire converged to a point to prevent DW nucleation. All structures were prepared on the same substrate during the same patterning and deposition stages to obtain nominally identical materials for all of the structures.

The nanowire designs included small amplitude sinusoidal edge modulations to both edges characterized by their wavelength, λ, and amplitude, A, as illustrated in Fig. 1. The values for wavelength range between 200 nm and 2 μm and the amplitudes between 15 nm and 50 nm.

In a second lithographic step, 16-μm-long, 2-μm-wide, 2.5-nm Cr/30-nm Au striplines were fabricated by thermal evaporation. These were positioned over the nanowire arrays with the two tapered ends and were perpendicular to the nanowire long axis. Further patterning of a larger 1-mm-wide pad allowed for electrical connections to co-axial cabling with conductive silver paint.

Magnetization reversal analysis was performed using a focused MOKE system with a beam footprint ≈10-μm wide to measure each array of nanowire structures. The change in the magnetization was measured in response to an axial magnetic field applied at 22 Hz, ± 270 Oe, which was quasistatic with respect to the pulsed magnetic fields from the stripline. The Kerr signal was averaged over ≈2500 field cycles to improve the signal-to-noise ratio, producing hysteresis loops of the magnetization behavior in the nanowires as a function of the magnetic field. The switching field from these loops was then found to within approximately 2 Oe and compared as a function of the edge-modulation parameters.

Additional localized pulsed magnetic fields from the stripline were used in combination with the quasistatic field to inject DWs into the nanowire structures at lower fields than was possible by DW injection from the geometrical nucleation pads. These pulsed fields were generated due to the Oersted field produced by the flow of a pulsed current through the stripline, produced from a pulser circuit consisting of a coaxial pulse-forming line that was discharged through the stripline into a 50-Ω load resistance. The pulse length was determined by the length of the pulse-forming line, the amplitude, from its initial charge voltage, and the pulse shape was monitored in real time throughout the investigation. The pulse triggering was synchronized with the quasistatic field, allowing the pulse to be triggered at various different quasistatic fields.

The DW propagation behavior in the nanowires was also investigated in longer 40-μm wires in order to investigate magnetic reversal behavior as a function of position along the nanowire, allowing the study of the propagation of a DW over a series of many wavelengths of edge modulation.

A detailed series of micromagnetic simulations and analyses were also performed using the OOMMF software package[31] on edge-modulated nanowire structures to aid the interpretation of the experimental results. These simulations used a 2-μm-long wire section with 500-nm tapered sections at both ends. The model geometries with both 5-nm and 10-nm thicknesses with a 250-nm average width were investigated as a function of their edge-modulation parameters. The simulations utilized a 5-nm mesh that is commensurate with the length scale of the exchange length for permalloy.[23] Typical micromagnetic material parameters for permalloy were used: $A = 13 \times 10^{-12}$ J/m, $M_s = 860 \times 10^3$ A/m, zero magnetocrystalline anisotropy, and a damping parameter, $\alpha = 0.5$, appropriate to the required quasistatic analysis.

III. RESULTS AND DISCUSSION

A. Modulation-based nucleation reversal behavior

First, results from the edge-modulated nanowire structures with two tapered ends are presented. Here the magnetization switching is governed by nucleation events within the modulated wire structure, giving rise to the magnetization reversal behavior shown by the examples in Fig. 2 for 35-nm edge-modulation amplitude and selected modulation wavelengths. These figures show a magnetization switching field dependence on the modulation parameters and also a variation in loop shape from sharper switching at longer wavelengths to more gradual magnetization reversal at low wavelengths.

The switching field extracted from these MOKE measurements and its dependence on the edge-modulation parameters is shown in Fig. 3. For long wavelength modulation, the nanowire can be approximated as an unmodulated wire giving

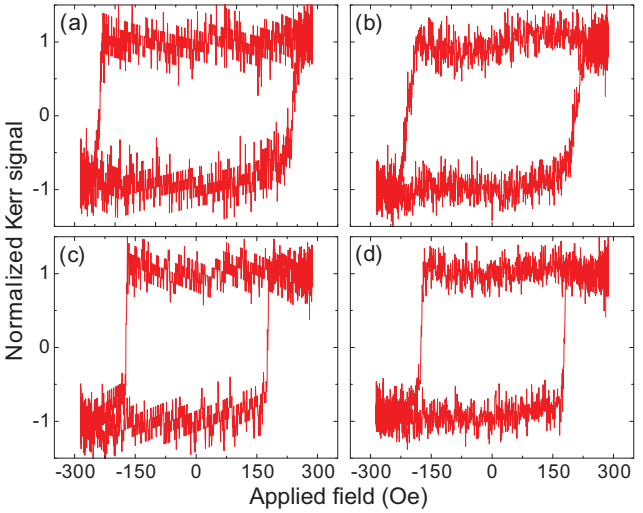

FIG. 2. (Color online) Example MOKE hysteresis loops for nanowires with two tapered ends, 35-nm modulation amplitude, and with wavelengths (a) 0.3 μm, (b) 0.4 μm, (c) 0.8 μm, and (d) 1.0 μm, where higher order magneto-optical effects have been removed.

a switching field largely independent of the modulation wavelength. As the wavelength is reduced, a gradual decrease in the switching field occurs down to a minimum before a steep increase is observed for the shorter wavelengths. This increase is observed up to the limit of the applied field, which corresponds to the shortest wavelengths reported in the figure. The modulation amplitude has little effect on the switching field for short wavelengths but leads to a reduced switching field for the larger amplitude wires with longer wavelength. The wavelength at which the minimum switching field occurs shifts toward larger values for increasing modulation amplitude.

Insight into the behavior of these edge-modulated nanowires has been achieved through the use of micromagnetic simulations where the wire structure was initially saturated in

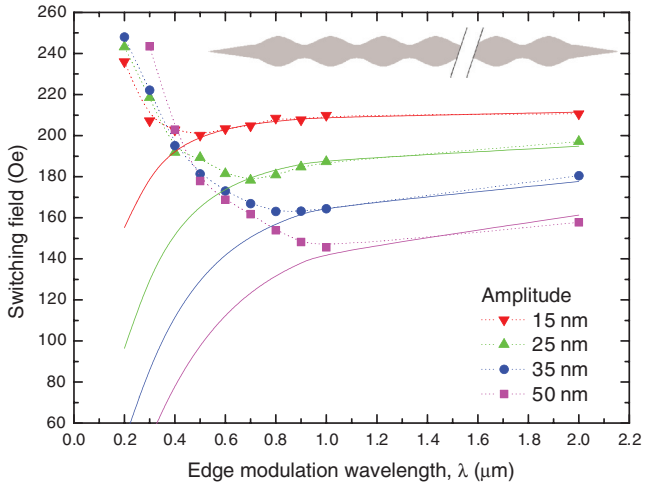

FIG. 3. (Color online) Magnetization switching field for edge-modulated nanowire structures with two tapered ends illustrated by the schematic insert, representing the variation in nucleation field with edge-modulation parameters. The solid line shows a fit of the model in the text to the long wavelength data.

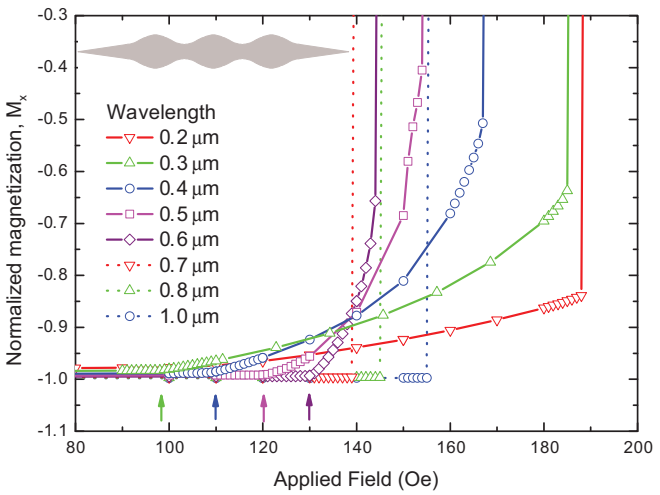

FIG. 4. (Color online) Sections from the region of increasing field of hysteresis loops from micromagnetic simulations on 5-nm-thick structures with 35-nm edge-modulation amplitude, illustrated by the schematic insert. A transition in switching behavior occurs between abrupt switching along wavelengths and magnetization rotation at shorter wavelengths.

the negative field direction and allowed to relax in zero field. An increasing positive axial field was then applied to the wire structure in 1 Oe steps until magnetization switching occurred. An example of the increasing field section of the hysteresis loops is shown in Fig. 4 for nanowires with 35-nm modulation amplitude and a thickness of 5 nm. This switching behavior is consistent with the MOKE results in Fig. 2, showing sharp switching between the two saturated states for longer wavelengths, while for shorter wavelengths the magnetization reversal is more complex. This consists of an initial gradual increase in magnetization with field followed by the sharp magnetization switching at a higher switching field.

The variation in the switching field obtained from the micromagnetic simulations as a function of edge modulation is shown by the solid symbols in Fig. 5, where the trend of the modeled behavior is very similar to that of the experimental results. There is little dependence of the switching field on wavelength for long wavelength modulation; the switching field decreases to a minimum before rising steeply in field as the wavelength is reduced. Again, the amplitude has little effect for short wavelengths but gives a reduced switching field for larger amplitude modulation at longer wavelengths. The simulations also agree with the experiments showing a shift in the minimum switching field toward longer wavelengths with an increase in modulation amplitude.

Significantly, the change in magnetization reversal behavior from sharp to gradual, seen in Fig. 4, occurs at a wavelength corresponding to the minimum in the switching field as a function of wavelength shown in Fig. 5. Further analysis of the micromagnetic simulated reversal for the shorter wavelength wires shows that the onset of the gradual increase in magnetization shifts toward lower values at shorter wavelengths, as is indicated by the arrows in Fig. 4. This reversal onset field is plotted as open symbols in Fig. 5 and reveals a continuous trend with the switching field results obtained for longer wavelength wires with the same amplitude. This suggests that both the full

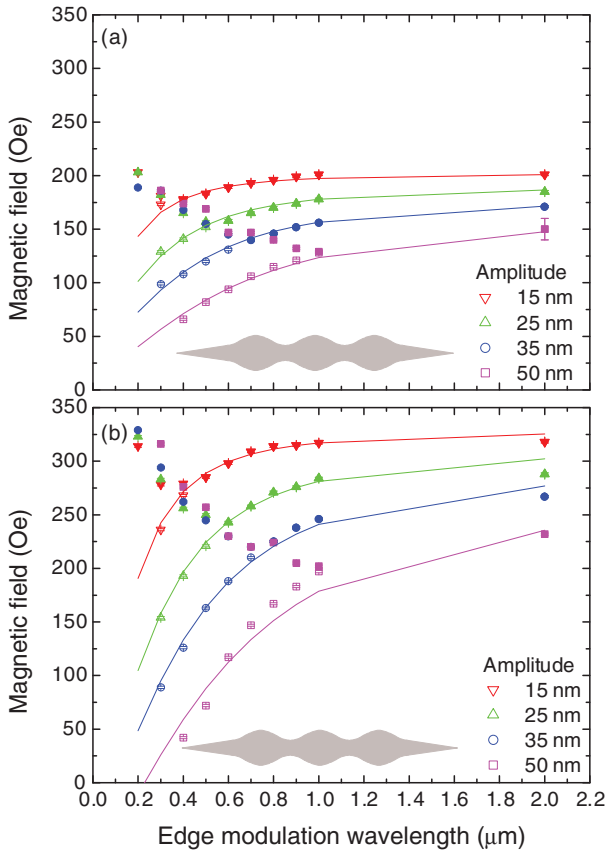

FIG. 5. (Color online) Micromagnetic simulations of (a) 5-nm-thick and (b) 10-nm-thick edge-modulated nanowire structures with two tapered ends, illustrated by the schematic insert. The switching field associated with the complete switching of the magnetization is represented by the solid symbols, and the open symbols show the field at which the onset of gradual magnetization rotation occurs for short wavelength modulation. The line shows a fit of the model in the text to the data.

switching field in longer wavelength structures and the reversal onset field at short wavelengths originate from the same physical phenomenon; this mechanism leads to a decrease in the reversal field with decreasing modulation wavelength. However, for the shorter wavelengths an additional effect dominates that gives rise to a steep increase in the switching field at low wavelengths.

The relationship between this decreasing trend in the reversal field with the modulation parameters has been explained here by developing a simplified analytical model based on the torque acting on the modulated spin structure due to the spin angle relative to the applied field along the axis of the wire. In unmodulated nanowires, the spins align parallel to the nanowire axis due to shape anisotropy effects. However, the inclusion of edge modulation gives rise to a local demagnetizing effect where spin alignment at the nanowire edges essentially tracks the contours of the edge modulation. With shorter wavelengths and larger amplitudes, the edge contours are steeper; hence, the spins at the nanowire edges are at a greater angle from the nanowire axis. The spins in the system experience a torque in a magnetic field given by $\boldsymbol{\tau} = \boldsymbol{m} \times \boldsymbol{B}$, which varies as the sine of the angle between the spin and applied field. The integral of this, $mB \int \sin\theta \, d\theta$, gives the energy associated with the rotation of the magnetic moment, $\boldsymbol{m}$, in a magnetic induction field, $\boldsymbol{B}$, giving a Zeeman energy barrier that scales as $-\cos\theta$ on top of a constant energy term associated with the rotation from orthogonal to parallel alignment. For small wavelength, large amplitude edge modulation, this gives a reduction in the Zeeman contribution to the energy barrier required for magnetization reversal and hence a decrease in the switching field.

For spins following the sinusoidal edge modulation with wavelength, λ, and amplitude, A, the maximum angle between the spin and applied field can be obtained from the maximum gradient of the edge modulation, $\arctan\left(\frac{2\pi A}{\lambda}\right)$. The energy considerations modify the energy barrier and lead to an expression for the reversal field, H_{rev}, expressed as

$$H_{\text{rev}} = A\gamma + \beta \cos\left(\arctan\left(\frac{2\pi\delta A}{\lambda}\right)\right). \qquad (1)$$

This includes a scaling factor, β, along with, $A\gamma$; to represent a modulation amplitude-dependent offset field term added to the switching field and an angular-scaling parameter, δ. This simplified expression was fitted to both the micromagnetic and long wavelength regions of the experimental datasets with β, γ, and δ as the free parameters, as shown by the solid lines plotted with the data in Figs. 3 and 5. For the experimental measurements on 10-nm-thick structures, the best fits gave values $\beta = 234 \pm 1$ Oe, $\gamma = -1.5 \pm 0.1$ Oe/nm, and $\delta = 1.8 \pm 0.1$. In comparison, fits to data extracted from micromagnetic simulations for 5-nm-thick wires gave values $\beta = 216 \pm 1$ Oe, $\gamma = -1.2 \pm 0.1$ Oe/nm, and $\delta = 1.9 \pm 0.1$, while for the 10-nm-thick wires the values were $\beta = 356 \pm 4$ Oe, $\gamma = -1.8 \pm 0.2$ Oe/nm, and $\delta = 2.7 \pm 0.1$.

The values of β include the switching-field dependence resulting from the average wire width and thickness; this increases in value for the thicker 10-nm-micromagnetic simulations and is consistent with higher switching fields expected for thicker nanowires. However, in the experimental data this parameter is lower than expected for the 10-nm sample. This difference may be due to the fabricational defects or roughness and small differences in magnetic parameters and may be also limited by stochastic thermal effects, which are not accounted for in the micromagnetic simulations. The other two parameters show similar values when fitted to the different datasets where γ shows a well-defined amplitude-dependent contribution. The δ factor acts as a correction to the ratio A/λ, and it is interesting to note that it takes the value $\delta \approx 2$, indicating that this modulation effect is actually governed by twice the ratio of A/λ for reasons that are not completely understood. Similarly, a factor of two also accounts for scaling of the minimum switching field where the minimum occurs at $\lambda/2A \approx 10$.

This model successfully accounts for the switching field dependence in the long wavelength regime; however, at shorter wavelengths an increase in the reversal field occurs due to the appearance of a gradual increase in the magnetization. Investigation of the spin configuration from micromagnetic simulations shows the origins of this magnetization increase. This is illustrated in Fig. 6 for the structure with $\lambda = 0.4$ μm, $A = 35$ nm, and 5-nm thickness with increasing applied

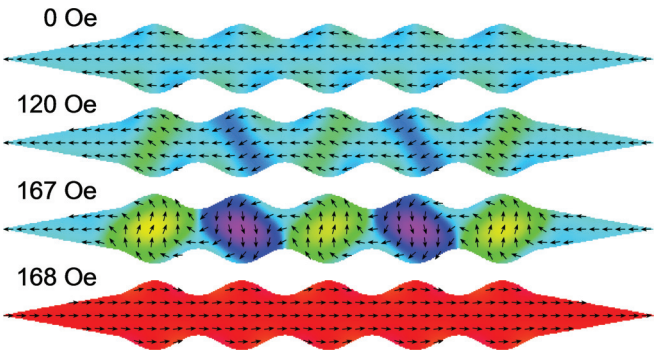

FIG. 6. (Color online) The micromagnetic spin structure simulated for edge-modulated structure with $\lambda = 0.4$ μm, $A = 35$ nm, and 5-nm thickness illustrated by the schematic insert. Increasing fields result in a spin rearrangement forming a stabilized state at intermediate fields leading to increased switching fields.

field that is representative of the behavior occurring for all structures below the minimum switching field. Initially, at zero field, the spins align largely along the nanowire axis with spins at the nanowire edges following the contours of the modulation, as described earlier. Increasing the field beyond the predicted switching field from the spin-angle model leads to the development of a spin state with magnetization components orthogonal to the wire axis in each lobe. The spins in these lobed regions continue to rotate with increasing field up until a switching field is exceeded (168 Oe in Fig. 6), when magnetization reversal is completed.

This spin structure develops with an orthogonal magnetization in the lobes due to the local shape anisotropy. In the case of large amplitude, short wavelength modulation, the lobes result in a localized decrease in axial shape anisotropy for the wire allowing lower total energy for this orthogonal magnetization state when in an applied magnetic field. To overcome the energy barrier, the switching requires a greater field; therefore, this orthogonal state acts to stabilize the magnetic spin structure in these wires, and the magnetization changes with field in a gradual, reversible way up to the increased switching field.

Interestingly, as shown in Fig. 6, the direction of the magnetization forms an alternating pattern from lobe to lobe. Although in some instances the initial direction may be set at multiple locations and lead to a sequence containing up-up or down-down magnetizations in adjacent lobes. These regions may give rise to a small energy contribution that is different from the case where all lobes alternate; however, this does not appear significant in determining the relevant switching fields explored here.

B. Modulation-based DW pinning and depinning behavior

In addition to understanding the influence of periodic structuring upon the direct nucleation of magnetization reversal, the behavior of magnetic DWs within these modulated structures was also investigated. In order to achieve this, structures were created to inject DWs into the modulated nanowires. First, nanowire structures with a nucleation pad were used to locally lower the nucleation field allowing a DW to be injected into the modulated nanowire.

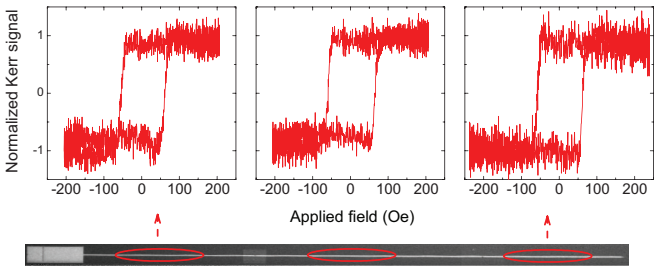

FIG. 7. (Color online) Experimentally measured magnetization switching at different locations along a 40-μm wire with $\lambda = 1.0$ μm and $A = 100$ nm. The magnetic switching behavior occurs at a consistent field along the whole length of the structure indicating DW propagation.

Initially, the uniformity of DW propagation was verified with a 40-μm-long nanowire allowing the magnetic switching behavior to be probed at several locations along the nanowire length. Figure 7 shows that a constant switching field was observed at several measurement positions along the wire, indicating that once a DW depins from one section of the modulated wire, the wall will propagate through all subsequent lobes along the wire at the same field.

The effect of the modulation parameters on the depinning, or propagation field for the DWs, was then investigated using arrays of 20-μm-long wires. The results are shown in Fig. 8 where DW mediated reversal allows for a reduction in the switching field in comparison to the same structures in Fig. 3. The open symbols in Fig. 8 show the reversal field obtained from MOKE measurements of these modulated structures; this represents the field at which a DW propagates along the nanowire. For long wavelengths the switching field is constant, showing no effect of the modulation wavelength or amplitude. However, toward shorter wavelengths, an increase

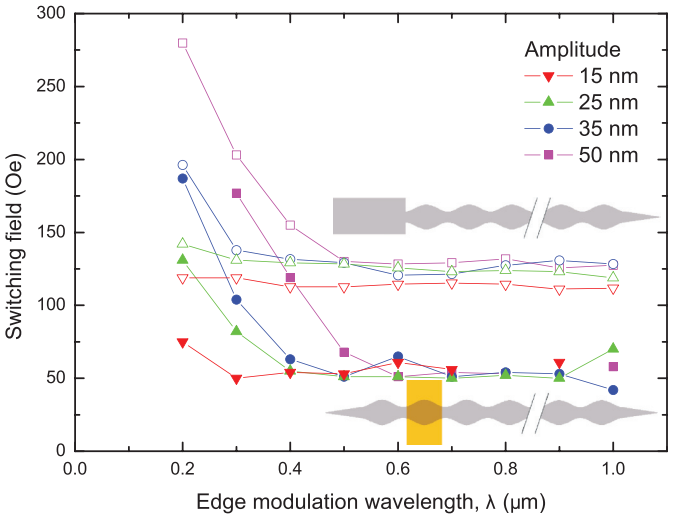

FIG. 8. (Color online) Experimentally measured switching field variation as a function of modulation wavelength and for different amplitudes, verifying the injection of DWs by nucleation pad (open symbols) and pulsed field (solid symbols). Below 125 Oe, switching fields are limited by injection from the nucleation pad. The wire structures are illustrated by the schematic inserts.

in the reversal field is observed, which is most significant for the structures with larger amplitude modulation.

The measured switching field here represents the field at which a DW successfully propagates along the nanowire structures. This is determined by a combination of the pad-injection field and the field for depinning a DW from the edge-modulated structure. The constant switching field for long wavelengths in Fig. 8 indicates that the behavior in this regime is actually limited by the field level required for DW injection from the nucleation pad and provides an upper limit on the DW propagation field in these modulated nanostructures.

To better understand the DW propagation field behavior in these structures, localized pulsed magnetic fields from a stripline were also used for the injection of DWs allowing for the investigation of DW properties at lower fields. The experimental reversal field behavior obtained using this technique is also shown in Fig. 8. Here, the solid symbols show that reversal occurs at lower fields, confirming that the previous measurements were pad-injection limited. The results, however, still show a switching field with constant behavior as a function of modulation parameters, again indicating the limits of this technique (the striplines are limited in current density and hence pulsed-field amplitude). Here the plateau represents the minimum quasistatic field required in combination with the maximum pulsed field amplitude to achieve DW formation and propagation. Further increase of the pulsed field amplitude for the $\lambda = 0.5\ \mu$m, $A = 25$ nm structure showed a further reduction in the reversal field to 21 Oe, but this ended with stripline burn-out due to heating effects. Shorter wavelengths show a similar increase in switching field, particularly for larger amplitude wires.

Domain wall depinning behavior was also investigated through micromagnetic simulations with an initial transverse DW structure in the center of the simulated wire structure. Again, the simulations involved applying an increasing axial field in 1 Oe steps until the DW depinned and led to the reversal of the magnetization of the wire. Figure 9 shows the results from these simulations for a variety of edge-modulation parameters. The results show similar trends to those observed in the experimental case, including low propagation fields for long wavelength modulation and an increase in propagation field for shorter wavelengths, which is also more significant for the larger amplitude modulation.

The presence of a DW allows the magnetization reversal to take place at lower fields compared to the earlier results for the direct nucleation-based field dependence. This is consistent with the commonly observed reversal behavior in unmodulated nanowires where switching by DW propagation occurs at the lower field.[11] Here the value of the propagation field is overestimated by the micromagnetic simulations for the ~10-nm-thick structures, which again accounted for differences in the edge roughness, material parameters, and thermal effects not accounted for in the modeling.

The micromagnetic simulations also give the spin structure of the DW in the modulated nanowire structure, providing insight into the origins of the behavior. Example sections from these simulations are shown in Fig. 10 for a modulated nanostructure with a wavelength $\lambda = 0.3\ \mu$m at zero field and at fields just below the DW depinning field. At zero field,

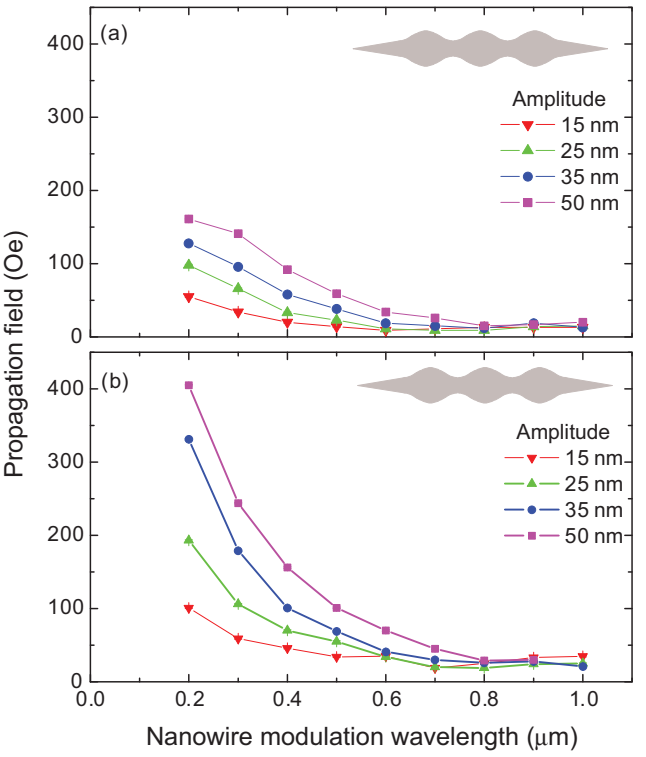

FIG. 9. (Color online) Switching field derived from micromagnetic simulations as a function of modulation wavelengths and for different amplitudes at (a) 5-nm and (b) 10-nm thickness.

the DW adopts an asymmetric transverse wall structure[32] with a reduced energy and extends across one of the lobed sections. The spin structure of this wall is then modified by the application of the axial magnetic field to a more symmetrical configuration before eventually depinning and propagating through the whole length of structure. For the largest amplitude modulation (50 nm), the DW actually shifts toward the constriction forming an additional state of reduced energy before the switching.

The structure of a DW depends on the relative contributions to the energy from the demagnetization and exchange terms. A DW pinned within an edge-modulated nanowire feels the

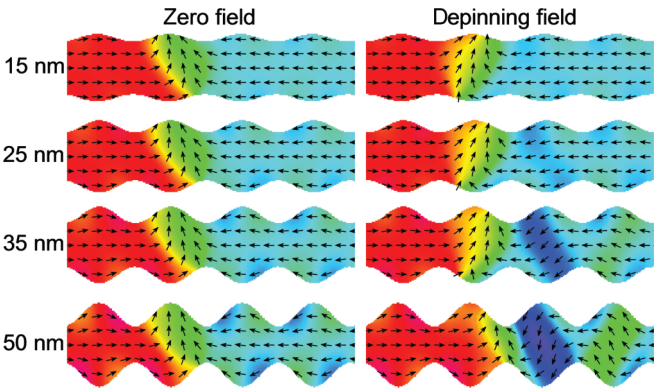

FIG. 10. (Color online) Simulations of the micromagnetic spin state at a field just before DW depinning for $\lambda = 0.3\ \mu$m wire at different amplitudes and 5-nm thickness.

effect of the periodic effective field; this has a reduced energy when the orthogonal component of magnetization of the DW is coincident with a wider lobe section. However, this results in the increase in the area of the DW with an increased exchange contribution. A minimum equilibrium energy configuration is established by the transition into an asymmetrical DW structure.[33–35]

The depinning field of the DW is determined by the pinning potential as a result of the DW structure and the local energetic landscape of the nanowire.[20] For magnetization reversal, the system must overcome an energy barrier associated with the rotation of the spins in the nanowire structure.[36] In the case of a modulated wire, an orthogonal magnetization component occurs in the lobes due to a localized reduction in the axial-shape anisotropy of the wire. This gives rise to a spatial dependence to the effective field,[25] leading to an alternating potential energy profile for a DW along the nanowire.[17]

The increase in the depinning field for nanowires with short wavelength and large amplitude results from a greater variation in the potential energy profile. If the orthogonal component of magnetization within each lobe is not parallel with the orthogonal magnetization of the DW, the spins must reorientate to overcome the localized shape anisotropy of the lobes, rotating back along the axis of the nanowire before undergoing the 180° spin rotation associated with the passage of the DW. Overcoming the localized shape anisotropy of the lobe gives rise to the observed increase in the depinning field.

For longer wavelengths, the regions of strong orthogonal magnetization do not develop as the axial shape anisotropy of the wire remains dominant. This explains why there is no wavelength dependence to the depinning field for longer wavelength modulation and the results more closely represent the behavior of unmodulated wires.

IV. CONCLUSIONS

The magnetization reversal behavior in edge-modulated nanowires was investigated as a function of sinusoidal edge-modulation parameters. This structuring affects the nucleation field shown by both experimental MOKE measurements and micromagnetic simulations. Here, a gradual decrease in switching field with reducing wavelength was explained by a simplified model based on the energy barrier associated with the torque on the spins following the edge contours of the modulated structures with respect to the field axis. This model shows the switching field scales in relation to the modulation parameters and shows good agreement with both experiment and micromagnetic results. For shorter wavelength, larger amplitude modulation, an additional magnetization reversal mode occurs where the spins rotate to a more energetically stable configuration. Here, the magnetization gains a significant component of magnetization orthogonal to the wire axis due to the local shape anisotropy; this results in an increase in the field required to first rotate the magnetization back along the nanowire axis before undergoing the 180° magnetization rotation associated with the propagation of a DW.

Magnetic DWs in these modulated nanostructures were investigated as a function of the modulation parameters showing, and they show a similar behavior to unmodulated wires where DW propagation occurs at a lower field compared to the nucleation field. This propagation field increases with short wavelength, large amplitude modulation as an effective field gives rise to an orthogonal magnetization providing a greater energy barrier, which needs to be overcome before successful switching takes place.

The results shown here provide valuable physical insight into the behavior of DWs in nanowire structures incorporating edge modulation. This may be useful for providing additional mechanisms for controlling DW behavior in future nanowire-based devices.

*Corresponding author: del.atkinson@durham.ac.uk

[1]S. S. P. Parkin, M. Hayashi, and L. Thomas, Science **320**, 190 (2008).
[2]D. Atkinson, D. S. Eastwood, and L. K. Bogart, Appl. Phys. Lett. **92**, 022510 (2008).
[3]H. Cramman, D. S. Eastwood, J. A. King, and D. Atkinson, IEEE Trans. Nano **11**, 63 (2012).
[4]D. A. Allwood, G. Xiong, C. C. Faulkner, D. Atkinson, D. Petit, and R. P. Cowburn, Science **309**, 1688 (2005).
[5]P. Vavassori, V. Metlushko, B. Ilic, M. Gobbi, M. Donolato, M. Cantoni, and R. Bertacco, Appl. Phys. Lett. **93**, 203502 (2008).
[6]M. Donolato, P. Vavassori, M. Gobbi, M. Deryabina, M. F. Hansen, V. Metlushko, B. Ilic, M. Cantoni, D. Petti, S. Brivio, and R. Bertacco, Adv. Mater. **22**, 2706 (2010).
[7]E. Rapoport and G. S. D. Beach, Appl. Phys. Lett. **100**, 082401 (2012).
[8]G. Ruan, G. Vieira, T. Henighan, A. Chen, D. Thakur, R. Sooryakumar, and J. O. Winter, Nano Lett. **10**, 2220 (2010).
[9]A. Torti, V. Mondiali, A. Cattoni, M. Donolato, E. Albisetti, A. M. Haghiri-Gosnet, P. Vavassori, and R. Bertacco, Appl. Phys. Lett. **101**, 142405 (2012).
[10]A. D. West, K. J. Weatherill, T. J. Hayward, P. W. Fry, T. Schrefl, M. R. J Gibbs, C. S. Adams, D. A. Allwood, and I. G. Hughes, Nano Lett. **12**, 4065 (2012).
[11]R. P. Cowburn, D. A. Allwood, G. Xiong, and M. D. Cooke, J. Appl. Phys. **91**, 6949 (2002).
[12]G. S. D. Beach, C. Nistor, C. Knutson, M. Tsoi, and J. L. Erskine, Nat. Mater. **4**, 741 (2005).
[13]E. B. Myers, D. C. Ralph, and J. A. Katine, Science **285**, 867 (1999).
[14]D.-S. Han, S.-K. Kim, J.-Y. Lee, S. J. Hermsdoerfer, H. Schultheiss, B. Leven, and B. Hillebrands, Appl. Phys. Lett. **94**, 112502 (2009).
[15]X. S. Wang, P. Yan, Y. H. Shen, G. E. W. Bauer, and X. R. Wang, Phys. Rev. Lett. **109**, 167209 (2012).
[16]C. C. Faulkner, M. D. Cooke, D. A. Allwood, D. Petit, D. Atkinson, and R. P. Cowburn, J. Appl. Phys. **95**, 6717 (2004).
[17]M. T. Bryan, T. Schrefl, and D. A. Allwood, Appl. Phys. Lett. **91**, 142502 (2007).
[18]D. A. Allwood, G. Xiong, and R. P. Cowburn, Appl. Phys. Lett. **85**, 2848 (2004).
[19]A. Himeno, T. Okuno, S. Kasai, T. Ono, S. Nasu, K. Mibu, and T. Shinjo, J. Appl. Phys. **97**, 066101 (2005).

[20]D. Lacour, J. A. Katine, L. Folks, T. Block, J. R. Childress, and M. J. Carey, Appl. Phys. Lett. **84**, 1910 (2004).
[21]A. Himeno, T. Ono, S. Nasu, K. Shigeto, K. Mibu, and T. Shinjo, J. Appl. Phys. **93**, 8430 (2003).
[22]M. Klaui, H. Ehrke, U. Rudiger, T. Kasama, R. E. Dunin-Borkowski, D. Backes, L. J. Heyderman, C. A. F. Vaz, J. A. C. Bland, G. Faini, E. Cambril, and W. Wernsdorfer, Appl. Phys. Lett. **87**, 102509 (2005).
[23]Y. Nakatani, A. Thiaville, and J. Miltat, Nat. Mater. **2**, 521 (2003).
[24]E. R. Lewis, D. Petit, L. O'Brien, A. Fernandez-Pacheco, J. Sampaio, A.-V. Jausovec, H. T. Zeng, D. E. Read, and R. P. Cowburn, Nat. Mater. **9**, 980 (2010).
[25]J. Ieda, H. Sugishita, and S. Maekawa, J. Magn. Magn. Mater. **322**, 1363 (2010).
[26]H. G. Piao, J. H. Shim, S. H. Lee, D. Djuhana, S.-K. Oh, S.-C. Yu, and D.-H. Kim, IEEE Trans. Magn. **45**, 3926 (2009).
[27]H. G. Piao, J. H. Shim, and D. Djuhana, IEEE Trans. Magn. **46**, 224 (2010).
[28]D. M. Burn and D. Atkinson, Appl. Phys. Lett. **102**, 242414 (2013).
[29]D. A. Allwood, G. Xiong, M. D. Cooke, and R. P. Cowburn, J. Phys. D: Appl. Phys. **36**, 2175 (2003).
[30]R. P. Cowburn, D. K. Koltsov, A. O. Adeyeye, and M. E. Welland, Appl. Phys. Lett. **73**, 3947 (1998).
[31]M. Donahue and D. Porter., The OOMMF code is available at http://math.nist.gov/oommf.
[32]Y. Nakatani, A. Thiaville, and J. Miltat, J. Magn. Magn. Mater. **290–291**, 750 (2005).
[33]D. Ravelosona, F. Cayssol, J. Wunderlich, H. W. Schumacher, C. Chappert, V. Mathet, J. Ferré, and J. P. Jamet, J. Magn. Magn. Mater. **249**, 170 (2002).
[34]J. Wunderlich, D. Ravelosona, C. Chappert, F. Cayssol, V. Mathet, J. Ferré, J. P. Jamet, and A. Thiaville, IEEE Trans. Magn. **37**, 2104 (2001).
[35]F. Cayssol, D. Ravelosona, C. Chappert, J. Ferré, and J. P. Jamet, Phys. Rev. Lett. **92**, 107202 (2004).
[36]Y. Yokoyama, Y. Suzuki, S. Yuasa, K. Ando, K. Shigeto, T. Shinjo, P. Gogol, J. Miltat, A. Thiaville, T. Ono, and T. Kawagoe, J. Appl. Phys. **87**, 5618 (2000).